Inorg. Chem. **2002**, *41*, 6573–6582

Inorganic Chemistry
Article

Bimetallic Carbonyl Thiolates as Functional Models for Fe-Only Hydrogenases

Frédéric Gloaguen, Joshua D. Lawrence, Thomas B. Rauchfuss,* Marc Bénard,† and Marie-Madeleine Rohmer†

Department of Chemistry, University of Illinois, Urbana, Illinois 61801, and Laboratoire de Chimie Quantique, UMR 7551, CNRS and Université Louis Pasteur, F-67000 Strasbourg, France

Received July 1, 2002

The anion $[Fe_2(S_2C_3H_6)(CN)(CO)_4(PMe_3)]^-$ (**2**$^-$) is protonated by sulfuric or toluenesulfonic acid to give $HFe_2(S_2C_3H_6)(CN)(CO)_4(PMe_3)$ (**2**H), the structure of which has the hydride bridging the Fe atoms with the PMe_3 and CN^- trans to the same sulfur atom. ^{1}H, ^{13}C, and ^{31}P NMR spectroscopy revealed that $HFe_2(S_2C_3H_6)(CN)(CO)_4(PMe_3)$ is stereochemically rigid on the NMR time scale with four inequivalent carbonyl ligands. Treatment of **2**$^-$ with $(Me_3O)BF_4$ gave $Fe_2(S_2C_3H_6)(CNMe)(CO)_4(PMe_3)$ (**2**Me). The Et_4NCN-induced reaction of $Fe_2(S_2C_3H_6)(CO)_6$ with $P(OMe)_3$ gave $\{Fe_2(S_2C_3H_6)(CN)(CO)_4[P(OMe)_3]\}^-$ (**4**). Spectroscopic and electrochemical measurements indicate that **2**H can be further protonated at nitrogen to give $[HFe_2(S_2C_3H_6)(CNH)(CO)_4(PMe_3)]^+$ (**2**H_2^+). Electrochemical and analytical data show that reduction of **2**H_2^+ gives H_2 and **2**$^-$. Parallel electrochemical studies on $[HFe_2(S_2C_3H_6)(CO)_4(PMe_3)_2]^+$ (**3**H^+) in acidic solutions led also to catalytic proton reduction. The **3**H^+/**3**H couple is reversible, whereas the **2**H_2^+/**2**H_2 couple is not, because of the efficiency of the latter as a proton reduction catalyst. Proton reduction is proposed to involve protonation of reduced diiron hydrides. DFT calculations establish that the regiochemistry of protonation is subtly dependent on the coligands but is more favorable to occur at the Fe–Fe bond for $[Fe_2(S_2C_3H_6)(CN)(CO)_4(PMe_3)]^-$ than for $[Fe_2(S_2C_3H_6)(CN)(CO)_4(PH_3)]^-$ or $\{Fe_2(S_2C_3H_6)(CN)(CO)_4[P(OMe)_3]\}^-$. The Fe_2H unit stabilizes the conformer with eclipsed CN and PMe_3 because of an attractive electrostatic interaction between these ligands.

Introduction

The reduction of protons to dihydrogen and the corresponding oxidation of dihydrogen to protons are processes of both fundamental and practical significance. Fundamental interest derives from the simple nature of the reactants. Proton reduction[1] is efficiently catalyzed by the hydrogenase enzymes (eq 1),[2−11] with rates up to 6000 turnovers per second quoted (30 °C).[12] Because of their efficiency, as well as the fact that they are not derived from expensive platinum metals, these enzymes provide an ideal opportunity to learn about the design of synthetic catalysts. High-resolution crystal structures of the two major families of hydrogenases (Fe-only[13−17] and NiFe[6,18]) encourage the rational design of catalyst candidates (Figure 1).

$$2e^- + 2H^+ \xrightleftharpoons{\text{hydrogenase enzymes}} H_2 \qquad (1)$$

In 1999, we reported that $[Fe_2(SR)_2(CN)_2(CO)_4]^{2-}$ (**1**) reacts with excess protic acids to give modest yields of H_2,

* To whom correspondence should be addressed. E-mail: rauchfuz@uiuc.edu.
† ULP, Strasbourg.

(1) Kubas, G. J. *Metal Dihydrogen and σ-Bond Complexes*; Kluwer Academic/Plenum Publishers: New York, 2001.
(2) Adams, M. W. W.; Morteson, L. E.; Chen, J. S. *Biochim. Biophys. Acta* **1981**, *594*, 105−176.
(3) Maroney, M. J.; Pressler, M. A.; Mirza, S. A.; Whitehead, J. P.; Gurbiel, R. J.; Hoffman, B. M. *Adv. Chem. Ser.* **1995**, *246*, 21−60.
(4) Pierik, A. J.; Hulstein, M.; Hagen, W. R.; Albracht, S. P. J. *Eur. J. Biochem.* **1998**, *258*, 572−578.
(5) Adams, M. W. W.; Stiefel, E. I. *Science* **1998**, *282*, 1842−1843.
(6) Fontecilla-Camps, J. C.; Ragsdale, S. W. *Adv. Inorg. Chem.* **1999**, *47*, 283−333.
(7) Adams, M. W. W.; Stiefel, E. I. *Curr. Opin. Chem. Biol.* **2000**, *4*, 214−220.
(8) De Lacey, A. L.; Stadler, C.; Cavazza, C.; Hatchikian, E. C.; Fernandez, V. M. *J. Am. Chem. Soc.* **2000**, *122*, 11232−11233.
(9) Ragsdale, S. W. *Subcell. Biochem.* **2000**, *35*, 487−518.
(10) Maroney, M. J.; Bryngelson, P. A. *JBIC, J. Biol. Inorg. Chem.* **2001**, *6*, 453−459.
(11) Siegbahn, P. E. M.; Blomberg, M. R. A.; Pavlov, M. W.; Crabtree, R. H. *JBIC, J. Biol. Inorg. Chem.* **2001**, *6*, 460−466.
(12) Adams, M. W. W. *Biochim. Biophys. Acta* **1990**, *1020*, 115−145.
(13) Peters, J. W.; Lanzilotta, W. N.; Lemon, B. J.; Seefeldt, L. C. *Science* **1998**, *282*, 1853−1858.
(14) Nicolet, Y.; Piras, C.; Legrand, P.; Hatchikian, C. E.; Fontecilla-Camps, J. C. *Structure* **1999**, *7*, 13−23.
(15) Lemon, B. J.; Peters, J. W. *Biochemistry* **1999**, *38*, 12969−12973.
(16) Lemon, B. J.; Peters, J. W. *J. Am. Chem. Soc.* **2000**, *122*, 3793−3794.
(17) Nicolet, Y.; de Lacey, A. L.; Vernède, X.; Fernandez, V. M.; Hatchikian, E. C.; Fontecilla-Camps, J. C. *J. Am. Chem. Soc.* **2001**, *123*, 1596−1601.

10.1021/ic025838x CCC: $22.00 © 2002 American Chemical Society
Published on Web 11/15/2002

Scheme 1. Formation of Hydride and Halide Bridged Species as Developed by Poilblanc et al.

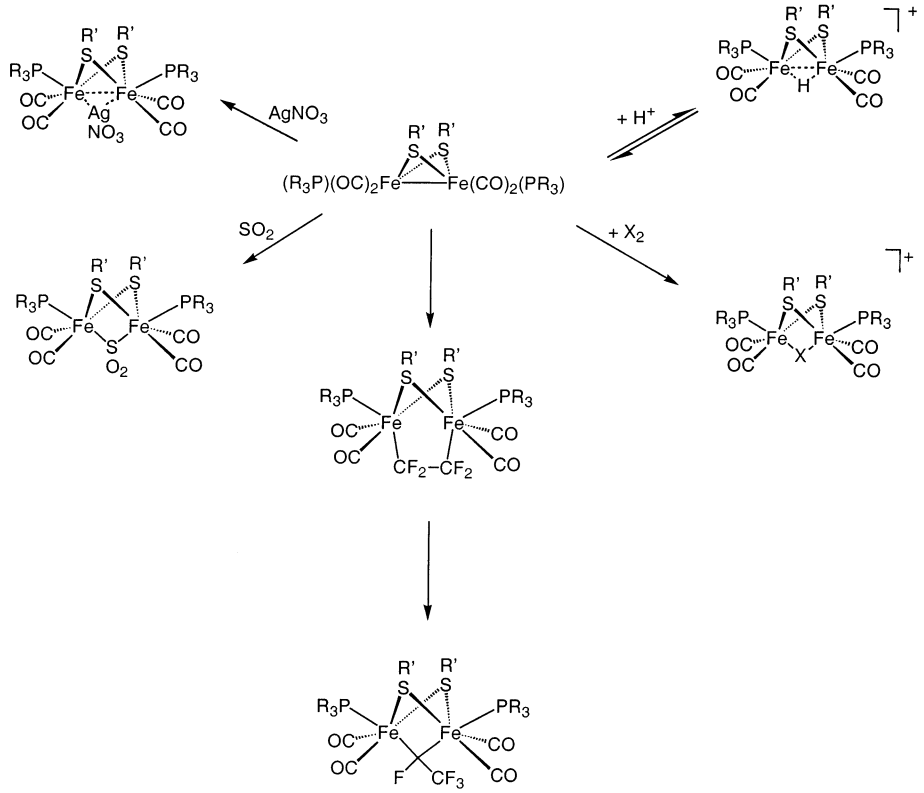

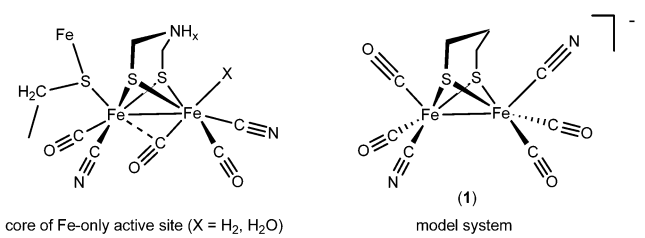

Figure 1. Active site of the Fe-only hydrogenase enzyme *Desulfovibrio desulfuricans* and the dicyano active site model.

but the diiron complex was irreversibly altered in the process.[19] We later found that the mixed ligand species $[Fe_2(S_2C_3H_6)(CN)(CO)_4(PMe_3)]^-$ (**2**$^-$) catalyzes the electroreduction of protons to dihydrogen.[20] In the present paper, we provide a more detailed description of **2**$^-$ and its derivatives and analogues as they relate to the proton reduction process, which is analyzed electrochemically and theoretically.

Our results are best viewed in relation to the salient features of complexes of the formula $[HFe_2(ER)_2(CO)_4L_2]^+$, where E = S, PR′, and L = PR″$_3$, which were studied extensively by Poilblanc et al. in the 1970s. The complexes $Fe_2(ER)_2(CO)_4(PR'_3)_2$ protonate at the Fe−Fe bond to give $[HFe_2(ER)_2(CO)_4(PR'_3)_2]^+$.[21−24] Oxidation of $Fe_2(ER)_2(CO)_4(PR'_3)_2$ with $AgPF_6$ or halogens (X = Cl, Br, I) gives $[XFe_2(ER)_2(CO)_4(PR'_3)_2]^+$ (Scheme 1).[25,26] Other electrophilic substrates add to the Fe−Fe bond including SO_2,[27,28] Ag^+,[25] and C_2F_4.[29]

Trialkylphosphine ligands greatly stabilize Poilblanc's hydrido complexes,[30] so it is logical that cyanide, which is a superior σ-donor ligand to PMe_3 (see Discussion), would also stabilize the hydrides. Indeed, treatment of $[Fe_2(SR)_2(CN)(CO)_4(PMe_3)]^-$ and $[Fe_2(SR)_2(CN)_2(CO)_4]^{2-}$ with acids gives $[HFe_2(SR)_2(CN)(CO)_4(PMe_3)]^-$ and $[HFe_2(SR)_2(CN)_2(CO)_4]^-$.[23]

Results

Protonation of $[Fe_2(S_2C_3H_6)(CN)(CO)_4(PMe_3)]^-$. Treatment of solutions of $[Fe_2(S_2C_3H_6)(CN)(CO)_4(PMe_3)]^-$ (**2**$^-$)[20] with protic acids in MeCN gave $HFe_2(S_2C_3H_6)(CN)(CO)_4(PMe_3)$ (**2**H), which precipitated upon the addition of H_2O. This μ-hydrido complex is moderately stable in solution and

(18) De Lacey, A. L.; Stadler, C.; Fernandez, V. M.; Hatchikian, E. C.; Fan, H.-J.; Li, S.; Hall, M. B. *JBIC, J. Biol. Inorg. Chem.* **2002**, *7*, 318−326.
(19) Schmidt, M.; Contakes, S. M.; Rauchfuss, T. B. *J. Am. Chem. Soc.* **1999**, *121*, 9736−9737.
(20) Gloaguen, F.; Lawrence, J. D.; Rauchfuss, T. B. *J. Am. Chem. Soc.* **2001**, *123*, 9476−9477.
(21) Le Borgne, G.; Grandjean, D.; Mathieu, R.; Poilblanc, R. *J. Organomet. Chem.* **1977**, *131*, 429−438.
(22) Fauvel, K.; Mathieu, R.; Poilblanc, R. *Inorg. Chem.* **1976**, *15*, 976−978.
(23) Zhao, X.; Georgakaki, I. P.; Miller, M. L.; Yarbrough, J. C.; Darensbourg, M. Y. *J. Am. Chem. Soc.* **2001**, *123*, 9710−9711.
(24) Savariault, J.-M.; Bonnet, J.-J.; Mathieu, R.; Galy, J. *C. R. Hebd. Seances Acad. Sci., Ser. C* **1977**, *284*, 663−665.
(25) Mathieu, R.; Poilblanc, R.; Lemoine, P.; Gross, M. *J. Organomet. Chem.* **1979**, *165*, 243−252.
(26) Haines, R. J.; de Beer, J. A.; Greatrex, R. *J. Chem. Soc., Dalton Trans.* **1976**, 1749−1757.
(27) Arabi, M. S.; Mathieu, R.; Poilblanc, R. *Inorg. Chim. Acta* **1979**, *34*, L207−L208.
(28) Taylor, N. J.; Arabi, M. S.; Mathieu, R. *Inorg. Chem.* **1980**, *19*, 1740−1742.
(29) Bonnet, J. J.; Mathieu, R.; Poilblanc, R.; Ibers, J. A. *J. Am. Chem. Soc.* **1979**, *101*, 7487−7496.
(30) Arabi, M. S.; Mathieu, R.; Poilblanc, R. *J. Organomet. Chem.* **1979**, *177*, 199−209.

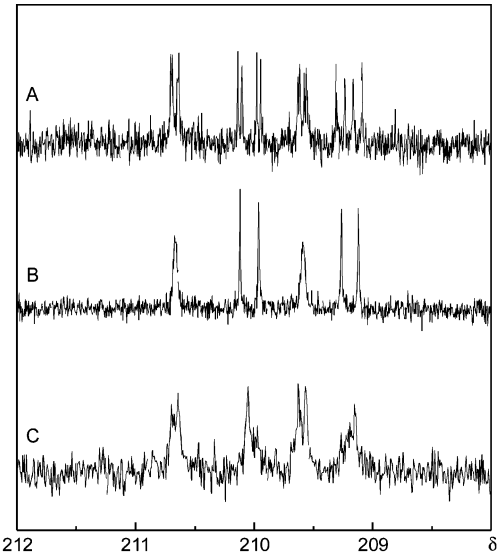

Figure 2. 126 MHz ^{13}C NMR spectra of the CO region of $HFe_2(S_2C_3H_6)(CN)(CO)_4(PMe_3)$ (**2**H) in CD_3CN: (A) no decoupling, (B) ^{1}H-decoupled, and (C) ^{31}P-decoupled.

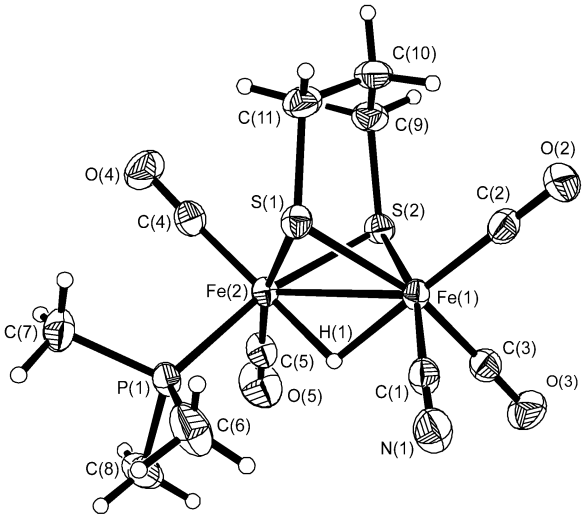

Figure 3. Thermal ellipsoid plot of $HFe_2(S_2C_3H_6)(CN)(CO)_4(PMe_3)$ (50% probability). The locations of the hydrogen atoms (including the hydride) were refined. Selected distances and angles are presented in Table 2.

in the solid state, although long-term storage required reduced temperatures. Reflecting its neutral character, **2**H is soluble in Et_2O, in contrast to (Et_4N)[**2**]; surprisingly, both (Et_4N)[**2**] and **2**H are soluble in aromatic solvents. In the ^{1}H NMR spectrum of **2**H, the signal for Fe_2H occurs as a doublet at δ −17 (J_{P-H} = 24 Hz) because of coupling to the PMe_3. The ^{31}P NMR spectrum also shows a doublet with the same coupling constant, which collapses to a broad singlet upon decoupling of the hydride ^{1}H NMR signal. Although a number of isomers are possible for **2**H, only one is observed in solution by ^{1}H and ^{31}P NMR spectroscopy.

The ^{13}C NMR spectrum of **2**H in the CO region consists of four signals with comparable intensity, two doublets and two doublets-of-doublets (Figure 2). The observed pattern arises from coupling of the hydride to all four CO ligands and the further coupling of the two CO ligands to PMe_3. The *C*N$^-$ signal is a broad singlet at −20 °C, but ^{13}C NMR *C*N signals of $[Fe_2(SR)_2(CN)_2(CO)_4]^{2-}$ compounds are frequently broadened, perhaps because of coupling to the quadrupolar ^{14}N. The hydride signal shows no coupling to the cyanide in 50% $^{13}CN^-$ enriched samples.

The Fe−Fe bond in (Et_4N)[**2**] is protonated by HCl (pK_a = 10.4 in MeCN[31−34]), but not by [*p*-$MeC_6H_4NH_3$]BF_4 (pK_a = 11.3 in MeCN[33]).[35,36] A pK_a value between 10.4 and 11.3 is comparable to that reported for $H_2Fe_3(CO)_9$(P-*t*-Bu) (pK_a = 11.4), but significantly less than that of (μ-H)$Fe_3(CO)_9$-(μ_3-S-C_6H_{11}) (pK_a = 16.9).[37] The deprotonation of **2**H is, however, sluggish because it resists deprotonation by NEt_3 (pK_a of $HNEt_3^+ \approx 18$).

Crystallographic characterization of $HFe_2(S_2C_3H_6)(CN)(CO)_4(PMe_3)$ (Figure 3) is fully consistent with the spectroscopy. Both PMe_3 and CN$^-$ ligands are trans to the same sulfur atom of the propanedithiolate ligand, giving an eclipsed or "cisoid" structure. The isomer observed for **2**H results from the protonation of one of the two isomers observed in the crystallographic analysis of (Et_4N)[**2**]. In the other isomer of (Et_4N)[**2**], the CN$^-$ is shifted trans to the Fe−Fe bond.[38] In the case of $Fe_2(SMe)_2(CO)_4(PMe_3)_2$ (where both thiolate-methyl groups are equatorial[39,40]), the phosphine ligands are trans to the Fe−Fe bond in the solid state. In a related protonated compound, $[HFe_2(SMe)_2(PMe_2Ph)_2(CO)_4](PF_6)$, crystallographic analysis shows both phosphine ligands trans to the bridging hydride.[24] Protonation elongates the Fe−Fe bond by approximately 0.05 Å in comparison to **2**$^-$, whereas the Fe−S, Fe−CO, and Fe−P distances are unaffected. The Fe−H distances are comparable to those of classical $[HFe_x(CO)_y]^-$ anions (for example, see $[HFe_2(CO)_8]^-$).[41] The bond distances, bond angles, and spectroscopic data are comparable to the two previously reported $HFe_2(SR)_2(CO)_4(L)(L')$ compounds that have been characterized spectroscopically and crystallographically (see Supporting Information).[23,24] The μ-hydride refined to a position that is unsymmetrical with respect to the Fe−Fe vector; unsymmetrical hydrides have been observed in other unsymmetrical bimetallic species.[42−46] The shorter bond is between H and the $Fe(PMe_3)$.

(31) Izutsu, K. *Acid−Base Dissociation Constants in Dipolar Aprotic Solvents*; Blackwell Scientific Publications: Oxford, 1990; Vol. 35.
(32) For mineral acids: Kolthoff, I. M.; Chantooni, M. K., Jr. *J. Chem. Eng. Data* **1999**, *44*, 124−129.
(33) For ammonium acids: Coetzee, J. F.; Padmanabhan, G. R. *J. Am. Chem. Soc.* **1965**, *87*, 5005−5010.
(34) $HClO_4$ = 1.6; $HOSO_2CF_3$ (HOTf) = 2.6; $HOSO_2C_6H_4CH_3$ (HOTs) = 8.0; HCl = 10.4; $H_3NC_6H_5^+$ = 10.6; H_4N^+ = 16.5.
(35) Moore, E. J.; Sullivan, J. M.; Norton, J. R. *J. Am. Chem. Soc.* **1986**, *108*, 2257−2263.
(36) Ededin, R. T.; Sullivan, J. M.; Norton, J. R. *J. Am. Chem. Soc.* **1987**, *109*, 3945−3953.
(37) Kristjansdottir, S. S.; Moody, A. E.; Weberg, R. T.; Norton, J. R. *Organometallics* **1988**, *7*, 1983−1987.
(38) Gloaguen, F.; Lawrence, J. D.; Schmidt, M.; Wilson, S. R.; Rauchfuss, T. B. *J. Am. Chem. Soc.* **2001**, *123*, 12518−12527.
(39) King, R. B. *J. Am. Chem. Soc.* **1962**, *84*, 2460.
(40) Maresca, L.; Greggio, F.; Sbrignadello, G.; Bor, G. *Inorg. Chim. Acta* **1971**, *5*, 667−674.
(41) Chin, H. B.; Bau, R. *Inorg. Chem.* **1978**, *17*, 2314−2317.
(42) Nataro, C.; Angelici, R. J. *Inorg. Chem.* **1998**, *37*, 2975−2983.
(43) Keijsper, J.; Grimberg, P.; Van Koten, G.; Vrieze, K.; Kojic-Prodic, B.; Spek, A. L. *Organometallics* **1985**, *4*, 438−446.

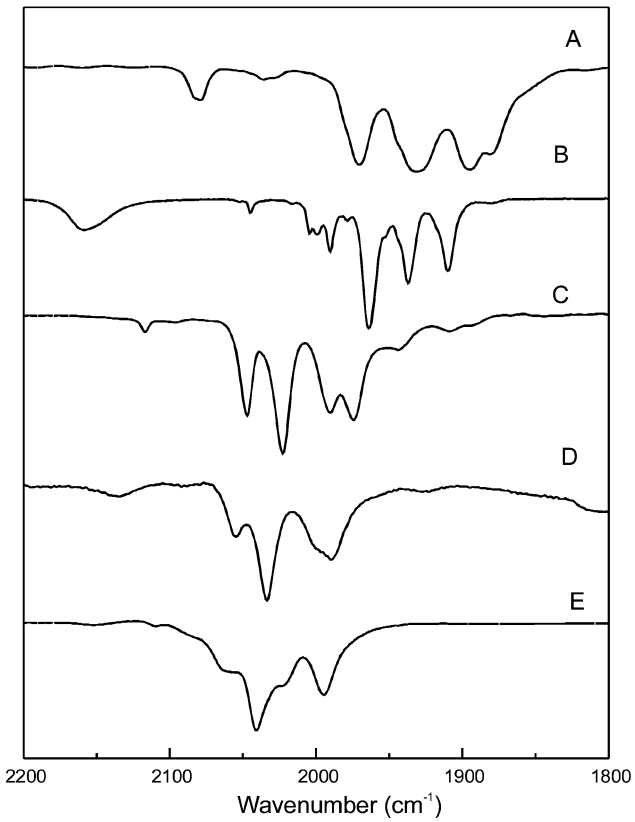

Figure 4. IR spectra of (A) $(Et_4N)[Fe_2(S_2C_3H_6)(CN)(CO)_4(PMe_3)]$ in MeCN, (B) $Fe_2(S_2C_3H_6)(CNMe)(CO)_4(PMe_3)$ in hexane, (C) $HFe_2(S_2C_3H_6)(CN)(CO)_4(PMe_3)$ in MeCN, (D) $[HFe_2(S_2C_3H_6)(CNH)(CO)_4(PMe_3)](OTs)$ in MeCN, and (E) $[HFe_2(S_2C_3H_6)(CNH)(CO)_4(PMe_3)](OTf)$ in MeCN.

The protonation of **2**H was further investigated because electrochemical experiments suggest that the doubly protonated complex is catalytically significant (see later).[20] The ν_{CO} bands shift approximately 10 cm^{-1}, and the ν_{CN} band disappears upon the addition of excess HOTf to MeCN solutions of **2**H. The collective evidence indicates that the second protonation gives the CNH complex $[HFe_2(S_2C_3H_6)(CNH)(CO)_4(PMe_3)]^+$ ($\mathbf{2}H_2^+$). The ν_{CNH} band is predicted[47] to occur between 2000 and 2030 cm^{-1} and may therefore be obscured by the ν_{CO} bands. Excess NEt_3 converts $\mathbf{2}H_2^+$ into **2**H but does not lead to the formation of $\mathbf{2}^-$ (see preceding description). HOTs, which in MeCN is 10^5 times less acidic than HOTf,[32] also causes the ν_{CN} to disappear, but the ν_{CO} bands only shift ~5 cm^{-1} (Figure 4). The fact that TsOH shifts ν_{CO} less than does HOTf is attributed to the occurrence of ion pairing between the Fe−CNH and OTs^-.[47]

Characterization of $Fe_2(S_2C_3H_6)(CNMe)(CO)_4(PMe_3)$, $Fe_2(S_2C_3H_6)(CO)_4(PMe_3)_2$, and $\{Fe_2(S_2C_3H_6)(CN)(CO)_4[P(OMe)_3]\}^-$ and Their Protonated Derivatives. Three analogues of $\mathbf{2}^-$ were examined in order to elucidate factors affecting proton reduction catalysis by **2**H. Methylation of $(Et_4N)[\mathbf{2}]$ with $(Me_3O)BF_4$ gave $Fe_2(S_2C_3H_6)(CNMe)(CO)_4(PMe_3)$ (**2**Me). The ^1H NMR spectrum of **2**Me shows signals for the phosphine (doublet) and isocyanide (singlet) ligands, as well as a well-resolved multiplet and doublet-of-triplets for the $(CH_2)_3$ of the propanedithiolate ligand. The ^{31}P NMR spectrum shows only one singlet. The IR spectrum of **2**Me in hexane in the ν_{CO} region is more complex than that of $\mathbf{2}^-$, which we attribute to the presence of conformers or decomposition.

Scheme 2. Dependence of the Regiochemistry of Protonation Versus Ancillary Ligand

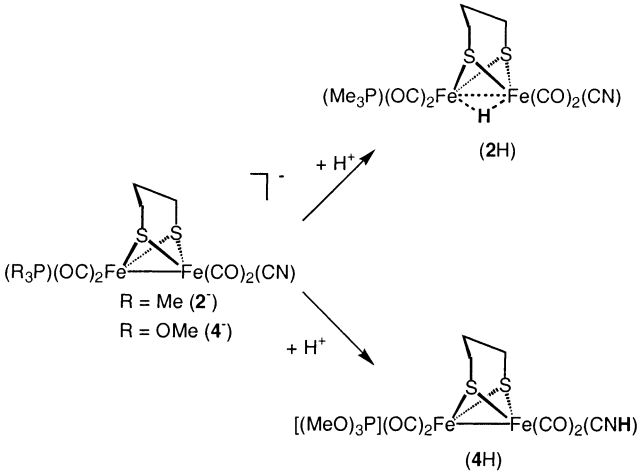

The diphosphine complex $Fe_2(S_2C_3H_6)(CO)_4(PMe_3)_2$ (**3**) is a close analogue of the species described by Poilblanc et al.[22,25,30] Protonation of **3** can be effected with HCl but not with toluidinium tetrafluoroborate, indicating the pK_a is approximately the same as that of $\mathbf{2}^-$ and probably similar to previously published analogues. The structure of the hydride complex was confirmed recently.[23]

The salt $(Et_4N)\{Fe_2(S_2C_3H_6)(CN)(CO)_4[P(OMe)_3]\}$ $(NEt_4)[\mathbf{4}]$ was synthesized by the reaction of Et_4NCN with $Fe_2(S_2C_3H_6)(CO)_6$ in the presence of $P(OMe)_3$ (eq 2). Spectroscopic characterization of this complex was straightforward. ^1H NMR spectra showed phosphite, dithiolate, and the tetraethylammonium counterion in a 1:1:1 ratio. The same pattern of bands in the IR spectrum was observed as for $(Et_4N)[\mathbf{2}]$, except that the ν_{CO} bands for $\mathbf{4}^-$ are ~15 cm^{-1} higher energy than for $\mathbf{2}^-$.

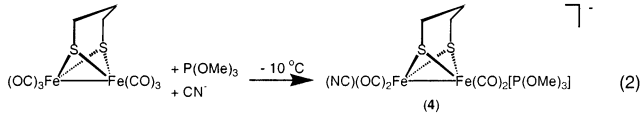

(2)

Treatment of $\mathbf{4}^-$ with HOTs results in protonation at CN^-, not at the Fe−Fe bond, as indicated by the modest shifts in ν_{CO} of 10−15 cm^{-1} (Scheme 2) and the lack of a ^1H NMR signal attributable to a hydride ligand. The change in the ν_{CO} bands induced by protonation in fact roughly matches that for **2**H versus $\mathbf{2}H_2^+$, which is 10 cm^{-1}. NMR analysis of in situ generated $Fe_2(S_2C_3H_6)(CNH)(CO)_4[P(OMe)_3]$ (**4**H) revealed the absence of hydride signal in the usual high field region. Protonation of both the CN moiety and the Fe−Fe

(44) Ashworth, T. V.; Liles, D. C.; Singleton, E. *J. Chem. Soc., Chem. Commun.* **1984**, 1317−1318.
(45) Johnson, B. F. G.; Lewis, J.; Pippard, D.; Raithby, P. R.; Sheldrick, G. M.; Rouse, K. D. *J. Chem. Soc., Dalton Trans.* **1979**, 616−618.
(46) Love, R. A.; Chin, H. B.; Koetzle, T. F.; Kirtley, S. W.; Whittlesey, B. R.; Bau, R. *J. Am. Chem. Soc.* **1976**, *98*, 4491−4498.
(47) Nataro, C.; Chen, J.; Angelici, R. J. *Inorg. Chem.* **1998**, *37*, 1868−1875.

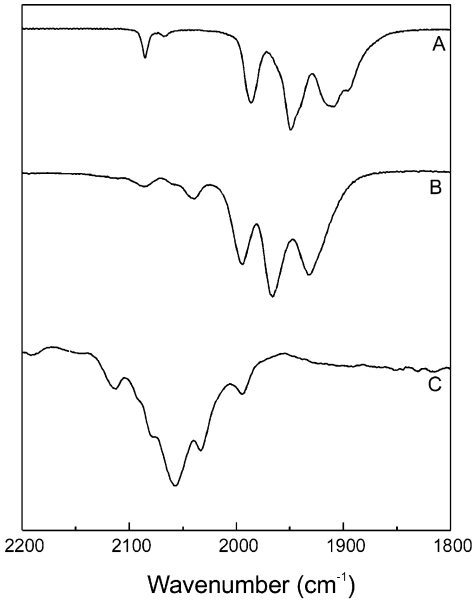

Figure 5. IR spectra of (A) $(Et_4N)\{Fe_2(S_2C_3H_6)(CN)(CO)_4[P(OMe)_3]\}$ in MeCN, (B) + 1 equiv HOTs in MeCN, (C) + excess HBF_4/Et_2O in MeCN.

bond in $\mathbf{4}^-$ to give $\{HFe_2(S_2C_3H_6)(CNH)(CO)_4[P(OMe)_3]\}^+$ with the strong acid HBF_4/Et_2O is indicated by shifts in the IR pattern (Figure 5), but the appearance of several weak signals in the hydride region in the ^{1}H NMR spectrum indicates that the resulting compound is unstable.

Redox Properties of $[HFe_2(S_2C_3H_6)(CN)(CO)_4(PMe_3)]$. The reduction of **2**H at $E_{1/2}^{red} = -1.13$ V, an apparent one-electron process ($\Delta E_p \sim 70$ mV at 200 mV s^{-1}), occurs at ~1 V milder than E_p^{red} for $\mathbf{2}^-$. The change in reduction potential upon protonation is typical.[48] The reduction of **2**H is not particularly well-behaved as it is followed by several smaller features in the range −1.5 to −2.0 V. Addition of 0.5 equiv of HOTs to a solution of **2**H gives a new species indicated by the appearance of a wave at $E_p^{red} = -0.98$ V (Figure 6b), assigned to the $\mathbf{2}H_2^+/\mathbf{2}H_2$ couple. On the second scan, the peak corresponding to the reduction of $\mathbf{2}H_2^+$ has disappeared, and the peak corresponding to the reduction of **2**H has increased, demonstrating the consumption of protons in the reduction. In the presence of excess acid, the $\mathbf{2}H/\mathbf{2}H^-$ reduction peak at $E_p^{red} = -1.13$ V is barely observable (Figure 6, curves a and b). The height of the reduction peak at ca. −1 V increases, and the potential shifts to a more cathodic value as the acid concentration increases (Figure 6, curves a−c). The shift in potential toward more negative potential is characteristic of a catalytic process.[49] We conclude that the reduction of $\mathbf{2}H_2^+$ is followed by chemical reactions in which proton consumption is relatively fast on the voltammetric time scale, that is, an EC catalytic process. Note also that upon reduction of $\mathbf{2}H_2^+$ no additional peaks are observed between −0.98 and −2.06 V (Figure 6, curve c), which indicates an efficient and well-behaved catalyst in

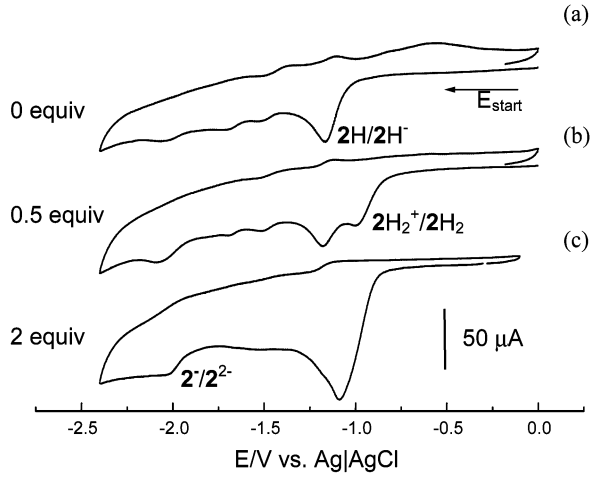

Figure 6. Cyclic voltammetry of a solution of 3 mM $[HFe_2(S_2C_3H_6)(CN)(PMe_3)(CO)_4] + x$ equiv HOTs: x = (a) 0, (b) 0.5, (c) 2. Conditions: 0.1 M Bu_4NPF_6 in MeCN, scan rate $v = 200$ mV s^{-1}, glassy carbon electrode of diameter 0.071 cm^2.

contrast to the behavior of **2**H, which exhibits several reductive processes (Figure 6, curve a).

Redox Properties of $[HFe_2(S_2C_3H_6)(CO)_4(PMe_3)_2]^+$ ($\mathbf{3}H^+$). It is useful to initially comment on the redox properties of $Fe_2(S_2C_3H_6)(CO)_4(PMe_3)_2$ (**3**) in the absence of protons. Characteristic of this class of diiron complexes, the diphosphine **3** is oxidized at mild potentials (0.24 V) and reduced irreversibly at highly negative potentials ($E_p^{red} = -1.87$ V). The oxidation appears somewhat reversible ($\Delta E_p \approx 70$ mV at 200 mV s^{-1}), although $(i_p^a/i_p^c)^{ox} < 1$.

Addition of HOTf or HOTs to a solution of **3** gives rise to new redox peaks attributed to the protonated complex $\mathbf{3}H^+$. As expected, the oxidation becomes more difficult by ~1.5 V ($E_p^{ox} = 1.6$ V) and almost completely irreversible. Reduction of $\mathbf{3}H^+$ generates some **3** ($E_p^{ox} = 0.24$ V), although the $\mathbf{3}H^+/\mathbf{3}H$ couple is at least partially reversible (in contrast to the irreversibility of $\mathbf{2}H_2^+/\mathbf{2}H_2$ couple).

Studies on the reduction of **3** in the presence of variable amounts of HOTs revealed that the reversibility (i_p^a/i_p^c for $E_{1/2}^{red} = -0.95$ V) decreases with [acid]/[**3**] (Figure 7). At [acid]/[**3**] > 3.6, reduction becomes completely irreversible, and the formation of **3** ($E_p = -0.3$ V), which was initially absent from the solution, becomes evident. Upon reduction of $\mathbf{3}H^+$, a small peak is also observed at ca. −0.3 V on the reverse scan, although the species responsible for this peak has not been identified. CV measurements reveal that proton reduction by $\mathbf{3}/\mathbf{3}H^+$ (eq 3) is competitive with reduction by

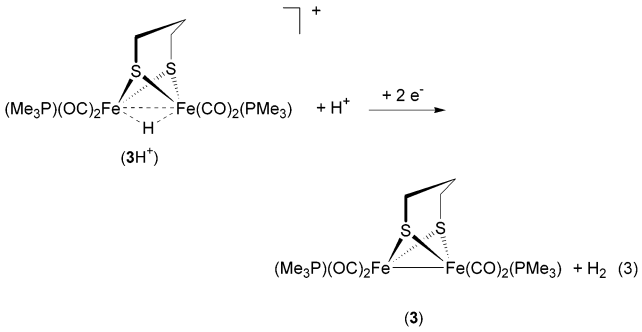

(48) Guedes da Silva, M. F. C.; Frausto da Sila, J. J. R.; Pombeiro, A. J. L.; Amatore, C.; Verpeaux, J. N. *NATO ASI Ser., Ser. C* **1993**, *385*, 483−487.

(49) Bhugun, I.; Lexa, D.; Savéant, J.-M. *J. Am. Chem. Soc.* **1996**, *118*, 3982−3983.

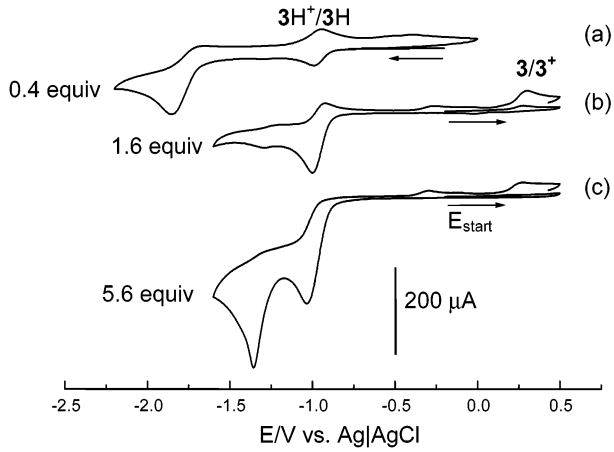

Figure 7. Cyclic voltammetry of a solution of $Fe_2(S_2C_3H_6)(CO)_4(PMe_3)_2$ ([**3**] = 3 mM) + x equiv of HOTs: x = (a) 0.4, (b) 1.6, (c) 5.6. See Figure 6 for conditions.

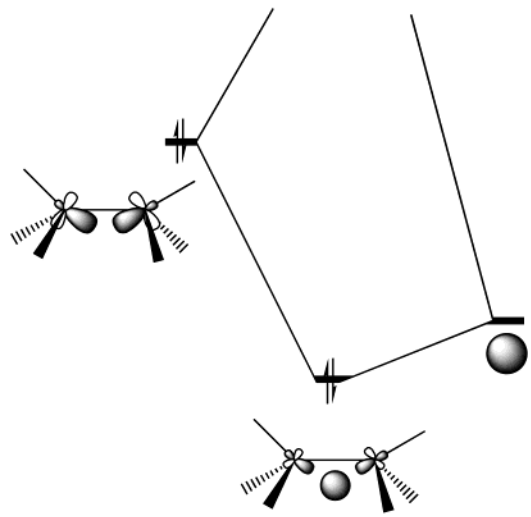

Figure 8. MO diagram of a protonated Fe−Fe bond.

the glassy carbon electrode (−1.4 V, see Figure 7 and Supporting Information Figure C). At similar [acid], reduction of free protons at the GC electrode was not observed in the presence of **2**H_2^+. The observation of a voltammetric peak for **3**/**3**$^+$ when [HOTs]/[**3**] ∼ 5.6 suggests that protonation is slow on the CV time scale (Figure 7, curve c).[32]

Redox Properties of [$HFe_2(S_2C_3H_6)(CNMe)(CO)_4(PMe_3)]^+$ (2MeH$^+$) and {$Fe_2(S_2C_3H_6)(CNH)(CO)_4[P(OMe)_3]$} (4H). Addition of HBF_4/Et_2O results in several new reduction peaks positive of the reduction of **4**$^-$ by ca. 1 V, but we observed no evidence for proton reduction comparable to that of **2**$^-$/**2**H_2^+ or even **3**/**3**H$^+$. Electrochemical measurements confirm that acids weaker than HBF_4 do not protonate **4**H at the Fe−Fe bond (see Supporting Information).

Upon addition of 1 equiv of HOTf to a solution of **2**Me, a new reduction peak due to the protonated complex is observed at E_p^{red} = −0.91 V, which is attributed to the **2**MeH$^+$/**2**MeH couple. Increasing acid concentration does not have a significant effect on the height of the reduction peak.

DFT Calculations on the Regiochemistry of Protonation. Calculations were aimed at (i) quantifying the energy difference between the various possible isomers of **2**H and (ii) analyzing the factors that influence the regiochemistry of protonation. At the outset, it is important to realize that protonation at Fe−Fe is orbitally driven (Figure 8), corresponding to formal oxidative addition, and differs strongly from protonation at C*N*, which is electrostatically driven. In the first case, the hydrogen atom is hydridic with a negative net charge, but it remains protic, with a positive charge in the latter case (Tables 2 and 3).[50] The structures and energetics of the four possible isomers of the protonated species **2**H, where protonation was considered at the bisector of the Fe−Fe bent bond or at C*N*, are displayed in Table 1. Two isomers, differing by a ∼120° rotation of the $Fe(CO)_2$(L) fragment, were considered for each protonated species. In the 0/0 isomer, the CN and PR_3 are eclipsed. This conformation corresponds to the crystal structure obtained for **2**H. A second conformation, referred to as 0/120, corresponds to the isomer where the P−Fe−Fe−C_N torsional angle is ∼120° (Tables 1 and 2). The relative energies of the four protonated isomers, Fe_2H (0/0), Fe_2H (0/120), H_{CN} (0/0), and H_{CN} (0/120), are relatively close for both R = H and R = Me, in keeping with the observed subtle dependence of the protonation regiochemistry on the coligands. The energy sequence for the four isomers changes when replacing PH_3 [H_{CN} (0/120) ≈ H_{CN} (0/0) < Fe_2H (0/0) < Fe_2H (0/120)] by PMe_3 [H_{CN} (0/120) ≈ Fe_2H (0/0) ≈ H_{CN} (0/0) < Fe_2H (0/120)].

The energy difference between H_{CN} (0/0) and H_{CN} (0/120) is only 1−2 kcal·mol^{-1}, (PR_3 = PH_3 or PMe_3) favoring the latter conformation. The C−N−H bond angle is predicted to be 131−136° in both cases. Such bent structures are observed in electron-rich isocyanide complexes,[51,52] whereas in **2**H_2^+ little back-bonding is expected. The actual structure of the FeCNH unit would be strongly influenced by nonbonding forces.

The relative energies of the two Fe_2H conformations follow an opposite trend, with the 0/0 form significantly more stable than the 0/120 conformation, especially with PMe_3 ($\Delta E_{0/120-0/0}$ = 4.5 kcal·mol^{-1}). The change in the energetic sequence for PH_3 versus PMe_3 arises from the more positively charged *P*Me_3, which interacts attractively with the cyanide ligand, thereby stabilizing the 0/0 conformer. In the crystal, the cyanide ligand is situated between PMe_3 ligands of two neighboring Fe_2H molecules. The attraction between the intermolecular phosphines and the cyanide ligand could explain the discrepancy between the experimental and theoretical values for Fe−Fe−C_{CN} angles and P···N distances (see Table 2). This trend is reversed when protonation occurs on nitrogen because CNH is slightly positive, with a charge

(50) Hirshfeld atomic charges are defined as $q_H = \int \rho_{mol}(r)^* \rho_{atom}(r) / \int \rho_{promol}(r)dr$ where $\rho_{atom}(r)dr$ is the density of an isolated atom in its ground state, $\rho_{mol}(r)$ is the calculated density in the molecule, and $\rho_{promol}(r)$ is the density generated by a "promolecule" made of the superposition of all noninteracting atoms. This definition yields atomic charges which are much more stable than Mulliken charges with respect to the basis set.

(51) Fehlhammer, W. P.; Fritz, M. *Chem. Rev.* **1993**, *93*, 1243−1280.
(52) Pombeiro, A. J. L.; Guedes da Silva, M. F. C.; Michelin, R. A. *Coord. Chem. Rev.* **2001**, *218*, 43−74.

Table 1. Structures of the 0/0 and 0/120 Conformations of $HFe_2(S_2C_3H_6)(CN)(CO)_4(PR_3)$ and of $Fe_2(S_2C_3H_6)(CNH)(CO)_4(PR_3)$ and Calculated Relative Energies (kcal·mol^{-1})

PR_3	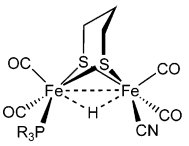 0/0 Fe_2H	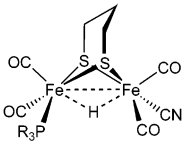 0/120 Fe_2H	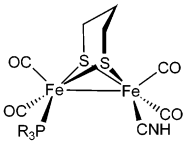 0/0 NH	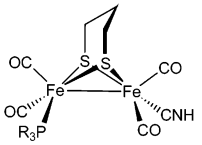 0/120 NH
PH_3	+5.7	+8.5	+1.3	0.0
PMe_3	+0.8	+5.25	+1.9	0.0
$P(OMe)_3$	+4.8	+4.4	+0.9	0.0

Table 2. Geometrical Parameters[a] and Hirshfeld Charges Calculated for $HFe_2(S_2C_3H_6)(CN)(CO)_4(PR_3)$ (R = H, Me, OMe)[50]

	R = H		R = Me			R = OMe	
	0/0[b]	0/120[c]	0/0	0/0 exptl	0/120	0/0	0/120
Fe−Fe	2.601	2.609	2.608	2.583	2.613	2.621	2.608
Fe(2)−H[d]	1.657	1.663	1.659	1.63	1.660	1.661	1.652
Fe(1)−H	1.687	1.695	1.687	1.70	1.692	1.714	1.710
Fe(2)−P	2.249	2.236	2.288	2.251	2.271	2.206	2.195
Fe(1)−C_{CN}	1.919	1.919	1.917	1.925	1.919	1.923	1.919
C−N	1.173	1.172	1.174	1.150	1.173	1.173	1.173
Fe−Fe−P	105.7	108.3	108.1	112.41	109.5	111.2	110.5
Fe−Fe−C_{CN}	102.6	105.9	103.2	111.59	105.1	109.0	105.1
P···H	2.57	2.60	2.62	2.63	2.59	2.62	2.59
P···N	3.87	5.70	4.01	4.67	5.61	4.52	5.70
Hirshfeld Charges							
Fe(2)	−0.09	−0.09	−0.09		−0.09	−0.10	−0.10
Fe(1)	−0.05	−0.05	−0.05		−0.05	−0.05	−0.05
H	−0.044	−0.044	−0.045		−0.046	−0.046	−0.045
P	+0.22	+0.22	+0.32		+0.31	+0.41	+0.41
PR[e]	+0.25	+0.24	+0.34		+0.34	+0.40	+0.39
PR_3	+0.29	+0.27	+0.36		+0.37	+0.33	+0.31
N	−0.30	−0.29	−0.29		−0.30	−0.30	−0.30
CN	−0.37	−0.37	−0.35		−0.38	−0.37	−0.38

[a] Distances in angstroms, angles in degrees. [b] PR_3 eclipsed with CN. [c] Torsional angle P−Fe−Fe−C_N = 120°. [d] PR_3 coordinated to Fe(2); CN coordinated to Fe(1). [e] R represents here the substituent closest to the hydride ligand.

Table 3. Geometrical Parameters and Hirshfeld Charges Calculated for $HFe_2(S_2C_3H_6)(CNH)(CO)_4(PR_3)$ (R = H, Me, OMe)[50]

	R = H		R = Me		R = OMe	
	0/0	0/120	0/0	0/120	0/0	0/120
Fe−Fe	2.577	2.568	2.592	2.589	2.588	2.592
Fe(2)−P	2.220	2.228	2.263	2.271	2.189	2.191
Fe(1)−C_{CN}	1.794	1.797	1.787	1.794	1.790	1.795
C−N	1.202	1.199	1.206	1.202	1.203	1.201
C−N−H	137.3	136.9	135.1	135.2	131.5	136.1
Fe−Fe−P	102.3	102.9	106.2	107.4	111.1	111.2
Fe−Fe−C_{CN}	103.8	101.5	106.1	102.0	105.5	103.5
P···N	3.95	5.36	4.25	5.52	4.39	5.72
Hirshfeld Charges						
Fe(2)	−0.12	−0.12	−0.11	−0.11	−0.17	−0.16
Fe(1)	−0.08	−0.08	−0.08	−0.08	−0.10	−0.09
P	+0.18	+0.19	+0.29	+0.29	+0.39	+0.39
PR_3	+0.19	+0.21	+0.27	+0.29	+0.21	+0.22
H	+0.16	+0.17	+0.16	+0.16	+0.15	+0.16
N	−0.16	−0.15	−0.16	−0.16	−0.16	−0.15
CNH	+0.04	+0.06	+0.03	+0.04	+0.03	+0.04

of +0.15 on the proton. The electrostatic interactions between PMe_3 and either CN^- or CNH correlate with the changes of the Fe−Fe−C_{CN} angles. Protonation at Fe−Fe leads to an increase of the Fe−Fe−C_{CN} angle in the 0/120 form (Table 2), but protonation at C*N* leads to diminished interligand *repulsion* in the 0/120 conformation and the angle evolves the opposite way (Table 3). As expected, the crystallographically confirmed structure of **3**H$^+$ is the 0/120 form,[23] resulting from a combination of steric and electrostatic repulsions between the phosphine ligands.

Protonation at the Fe−Fe bond also establishes an attractive interaction between the positive phosphorus atom and the hydride ligand. However, the nature of the phosphine substituent R is also a key factor in determining the strength of this interaction, primarily because R modulates the donor strength of PR_3 and therefore influences the charge at P. Extended Hückel calculations show that the lone pair orbital of PR_3 is higher by 1.4 eV for R = Me (−13.14 eV) than for R = H (−14.53 eV). Because the lone pair of PMe_3 interacts more strongly with Fe, the P in the coordinated PMe_3 is more positively charged than is coordinated PH_3. The strong Fe−P interaction in **2**H therefore explains the relative stabilization of both Fe_2H isomers with respect to the N-protonated forms. Furthermore, the enhanced energy gap between the 0/0 and the 0/120 forms of $HFe_2(S_2C_3H_6)(CN)(CO)_4(PR_3)$ of 4.45 kcal·mol^{-1} for R = Me versus 2.8 kcal·mol^{-1} for R = H (see Table 1) is also in agreement with a stronger PMe_3−cyanide attraction.

The interligand electrostatic interactions are more complex with the $P(OMe)_3$ bearing **4**. The phosphorus atom and the whole $P(OMe)_3$ ligand still keep an important positive charge. However, in the μ-H protonated forms, the lone pairs of two of the oxygen atoms strongly interact with the hydride, and also with nitrogen in the 0/0 conformation. Consequently, this conformer is not stabilized with respect to the 0/120 form as for the phosphine complexes, and both μ-H forms remain destabilized by ∼4 kcal·mol^{-1} compared to the CNH isomers.

The structural differences in the complex core are surprisingly small between the various isomers of the protonated complex, especially between the Fe_2H and the CNH isomers. The most obvious consequence of protonation on N is the shortening of the Fe(1)−CN distance by ∼0.13 Å, again consistent with increased Fe−C_N back-bonding (Table 3).

Discussion

Protonation of $[Fe_2(S_2C_3H_6)(CN)(CO)_4(PMe_3)]^-$, **2**$^-$, to give the hydrido complex **2**H was anticipated by the extensive studies of Poilblanc, which demonstrated the basicity of the diiron unit. What was less obvious was that protonation at the FeFe bond would be competitive with

protonation at C*N*. The protonation of almost all metal cyano complexes occurs at C*N*, not M.[47,53] The most basic site in $[Fe_2(S_2C_3H_6)(CN)_2(CO)_4]^{2-}$ is the diiron center, although the resulting $[HFe_2(S_2C_3H_6)(CN)_2(CO)_4]^-$ is unstable.[23] The sensitive energetic balance that regulates the relative basicity of the Fe−Fe bond versus C*N* is illustrated by the fact that the $P(OMe)_3$ analogue of $\mathbf{2}^-$, $[Fe_2(S_2C_3H_6)(CN)(CO)_4(P(OMe)_3)]^-$, protonates at C*N*$^-$. The DFT calculations also point to a subtle energetic balance. The hydrido complexes $HFe_2(S_2C_3H_6)(CN)(CO)_4(PMe_3)$ (**2**H) and $[HFe_2(S_2C_3H_6)(CO)_4(PMe_3)_2]^+$ ($\mathbf{3}H^+$) are spectroscopically similar. In terms of structure, these two species differ in terms of the relative positions of the donor ligands, which can be rationalized by DFT studies, but the energy differences between such isomeric species has been calculated to be small.

The proton reduction efficiencies of $\mathbf{2}H_2^+$ versus $\mathbf{3}H^+$ differ significantly, which is interesting because the difference points to a possible functional role for CN, a common component in the two major families of hydrogenase enzymes.[7] Several indicators suggest that the $\mathbf{3}/\mathbf{3}H^+$ pair is less catalytically active than the $\mathbf{2}^-/\mathbf{2}H_2^+$ pair: (i) Reduction of $\mathbf{3}H^+$ is partially reversible, indicating that the reduced hydride is less reactive toward protons than is the corresponding cyano−hydride **2**H. (ii) Upon reduction of $\mathbf{3}H^+$ in the presence of excess H^+, **3** is always detected on the reverse scan, indicating that it protonates relatively slowly (on the seconds time scale).[54] (iii) The height of the wave for the reduction of $\mathbf{3}H^+$ is only moderately responsive to $[H^+]$. (iv) Reduction of protons by **3** is competitive with proton reduction at the glassy carbon electrode, whereas it is not for **2**H.

Chemical and electrochemical experiments support a mechanism that begins with the protonation at the diiron unit, the reduction product of which interacts with a second proton (EC mechanism). This mechanism for proton reduction was previously elucidated by Koelle for $CpCo(PR_3)_2$-based electrocatalysts.[54] Savéant has demonstrated the converse, that proton reduction catalysis with metalloporphyrins is initiated by reduction of the catalyst *followed* by protonation.[49] In terms of a more intimate mechanism for the proton reduction, we propose that hydrogen evolution occurs upon reduction of the doubly protonated complex $\mathbf{2}H_2^+$ to the mixed valence hydride, $[H(Fe^{1.5})_2(S_2C_3H_6)(CNH)(CO)_4(PMe_3)]^0$, followed by heterolytic hydrogen formation. An enticing hypothesis is that the greater efficiency of the cyanide−phosphine versus the diphosphine is due to the intramolecular coupling of the hydridic (Fe_2*H*) and protic (FeCN*H*) centers in $\mathbf{2}H_2^+$ (see point iii in preceding paragraph). Furthermore, the kinetically facile protonation of FeC*N* may serve as a proton relay to the diiron center (see point ii in preceding paragraph). Scheme 3 presents a unified mechanism for hydrogen production by $\mathbf{2}^-$ and **3**. It should be noted that, in the H_2 formation step, the cyanide system ($\mathbf{2}H_2$) does not require an external acid source, which could increase the rate of proton reduction.

Scheme 3. Proposed Mechanism of Hydrogen Evolution

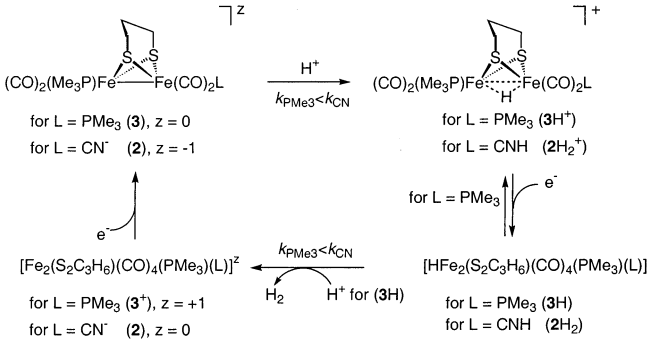

Table 4. Tolman Parameters

	CN^-	PMe_3	CNMe	$P(OMe)_3$
Tolman parameter ν (cm^{-1})	−11.1[57]	8.0[55]	17[56]	23.4[55]

Table 5. Additive Tolman Parameters

	$CN^- + CN^-$	$CN^- + PMe_3$	$PMe_3 + PMe_3$	$CNMe + PMe_3$	$CN^- + P(OMe)_3$
additive Tolman param $\Sigma\nu$ (cm^{-1})	−22.2	−3.1	16	25	12.3
$E_p{}^a$ (mV) for Fe_2^{2+}/Fe_2^{3+} in MeCN	−80	50	240	410	270

The basicity of the diiron unit correlates with catalysis. For this analysis, it is helpful to review the donor properties of the ancillary ligands that were varied in this study, PMe_3, MeNC, CN^-, and $P(OMe)_3$. Tolman has previously proposed a useful semiquantitative assessment of the σ-donor properties of ligands (Table 4) based on the IR properties of their $Ni(CO)_3$ derivatives.[55] For ease of comparison, ν is taken to be the difference between the A_1 band of $Ni(CO)_3L$ and that of $Ni(CO)_3(P^tBu_3)$, e.g., $\nu(P^tBu_3) = 0$. The complex $[Ni(CO)_3(CN)]^-$ has subsequently been characterized,[57] which allowed an extension of Tolman's analysis to cyanide, although solvation effects become more important for this ligand. This analysis indicates that CN^- is significantly more basic than PMe_3. The difference between PMe_3 and $P(OMe)_3$, which are considered to have disparate donor properties, is less than the difference between CN^- and PMe_3. Using the expanded Tolman parameters, one can then compare the five complexes discussed in this paper in terms of their ligand additivity effects (Table 5), $\sum\nu$. These species exhibit the following ranking: $(CN^-)_2 < [(CN^-)(PMe_3)] < [(CN^-)(P(OMe)_3)] < (PMe_3)_2 < [(CNR)(PMe_3)]$. This same trend is followed in terms of the redox potentials (in the absence of protons). As expected, CN^- has a dominating influence on both trends. In the presence of protons, the order is complicated by the fact that the cyanide−phosphite (but not the cyanide−phosphine or the dicyanide) protonates first at the cyanide. The donor ability of CNH is probably comparable to that of CNMe, or weaker. Parallel experiments on $\{Fe_2(S_2C_3H_6)(CN)(CO)_4L\}^-$ (L = PMe_3 and $P(OMe)_3$) show that the less basic $P(OMe)_3$ derivative is not active for proton reduction catalysis. This result can be rationalized within the

(53) Bianchini, C.; Laschi, F.; Ottaviani, M. F.; Peruzzini, M.; Zanello, P.; Zanobini, F. *Organometallics* **1989**, *8*, 893−899.
(54) Koelle, U.; Paul, S. *Inorg. Chem.* **1986**, *25*, 2689−2694.
(55) Tolman, C. A. *J. Am. Chem. Soc.* **1970**, *92*, 2953−2956.
(56) Haas, H.; Sheline, R. K. *J. Chem. Phys.* **1967**, *47*, 2996−3022.
(57) Joo, F.; Alper, H. *Organometallics* **1985**, *4*, 1775−1778.

context of a mechanism whereby H_2 formation occurs via protonation at an iron hydride, the basicity of which is regulated by the ancillary ligands.

Summary

The complex $Fe_2(CO)_4(S_2C_3H_6)(CN)(PMe_3)$ provides the interesting case of a dinuclear system in which the changing of substituents in a ligand that could be a priori considered as innocent (H vs Me vs OMe) is capable of inducing a major modification of the chemical behavior affecting the electronic structure of the molecular core, and especially the metal−metal bond. This exaggerated response of the system appears as a consequence of the delicate energetic balance that exists between two strikingly different protonation pathways, a singularity of this class of molecules.

It is intriguing that proton reduction is efficiently catalyzed by a complex that is structurally related to the Fe-only hydrogenase active site.[58,59] In the enzyme, it is proposed that the proton reduction occurs via a terminal iron hydride, whereas our catalyst enters the catalytic cycle with a bridging hydride, as verified crystallographically and spectroscopically. If the proposed terminal hydride mechanism is true, then a major challenge for this area of biomimetic catalysis is to synthesize electroactive diiron models with terminal hydride ligands. In such a case, one again would need to balance protonation at Fe versus C*N*.

Experimental Section

General Procedures. Organosulfur and organophosphorus compounds, Et_4NCN, and $Fe(CO)_5$, were obtained from Aldrich and used without further purification. Compounds $Fe_2(S_2C_3H_6)(CO)_4(PMe_3)_2$ (**3**) and $[Fe_2(\mu\text{-}H)(S_2C_3H_6)(CO)_4(PMe_3)_2](PF_6)$ (**3**H^+) were prepared by literature methods.[21−24] Solvents were purified by degassing with a nitrogen purge and were dispensed through two 1-m long columns of active alumina. Reactions were carried out under an atmosphere of purified nitrogen using either standard Schlenk techniques or an inert atmosphere glovebox.

$Fe_2(S_2C_3H_6)(CO)_6$ was prepared by a minor variation of the literature method[60] as follows: a suspension of 1.5 g of $Fe_3(CO)_{12}$ in 100 mL of toluene was treated with 1 equiv of 1,3-propanedithiol. The reaction mixture was stirred at 80 °C until its color changed from deep green to dark red. The reaction mixture was allowed to cool to room temperature and filtered. The red filtrate was evaporated to dryness under vacuum, and the residue was extracted with 3 × 10 mL of hexanes. The combined solution was filtered through a silica column (20 × 3 cm). The volume of the filtrate was reduced under vacuum to ca. 5 mL and cooled to −20 °C to give red crystals of $Fe_2(S_2C_3H_6)(CO)_6$. Yield: 65−80%.

Electrochemistry. Cyclic voltammetry experiments were carried out in a ca. 5-mL one-compartment glass cell. The working electrode was a glassy carbon disk (0.3 cm in diameter), the reference electrode an Ag|AgCl electrode (ca. −0.40 V vs Fc/Fc^+), and the counter electrode a Pt wire. The electrolyte was 0.1 M Bu_4NPF_6 in MeCN. The typical concentration of the organometallic complex was ca. 3 mM. The acid concentration in the electrolyte was varied by addition of measured volumes (ca. 50 μL) of a solution of either HOTs or CF_3SO_3H in MeCN.

Table 6. Details of Data Collection and Structure Refinement for **2H**

chemical formula	$C_{11}H_{16}Fe_2NO_4PS_2$
temp (K)	193(2)
cryst size (mm^3)	0.40 × 0.24 × 0.10
space group	$P2_1/c$
a (Å)	14.126(6)
b (Å)	9.143(4)
c (Å)	13.749(6)
α (deg)	90
β (deg)	105.027(7)
γ (deg)	90
V ($Å^3$)	1715.0(12)
Z	4
D_{calcd} (Mg m^{-3})	1.677
μ (Mo Kα, mm^{-1})	0.71073
max/min trans	0.9982/0.7160
reflns measd/indep	14923/4147
data/restraints/params	4147/0/254
GOF	1.076
R_{int}	0.0312
R1[a] [$I > 2\sigma$] (all data)	0.0231 (0.0310)
wR2[b] [$I > 2\sigma$] (all data)	0.0571 (0.0562)
max peak/hole ($e^-/Å^3$)	0.363/−0.283

[a] $R1 = \sum||F_o| - |F_c||/\sum|F_o|$. [b] $wR2 = \{\sum[w(F_o^2 - F_c^2)^2]/\sum[w(F_o^2)^2]\}^{1/2}$.

Crystallography. Crystals were mounted to a thin glass fiber using oil (Paratone-N, Exxon). Data were filtered to remove statistical outliers. The integration software (SAINT) was used to test for crystal decay as a bilinear function of X-ray exposure time and sine(θ). Data were collected at 198 K on a Siemens CCD diffractometer. Crystal and refinement details are given in Table 6. The structures were solved using SHELXTL by direct methods; correct atomic positions were deduced from an *E* map or by an unweighted difference Fourier synthesis. H atom *U*s were assigned as 1.2 times the U_{eq}'s of adjacent C atoms. Non-H atoms were refined with anisotropic thermal coefficients. Successful convergence of the full-matrix least-squares refinement of F^2 was indicated by the maximum shift/error for the last cycle.

Computational Details. Calculations were carried out using the formalism of the density functional theory (DFT) within the generalized gradient approximation (GGA), as implemented in the ADF program.[61−64] The exchange-correlation functional used in the calculations is currently referred to as BP86. In this formalism, nonlocal corrections of Becke for the exchange energy[65,66] and of Perdew for the correlation energy[67,68] have been added to the standard local spin density functional based upon the electron gas exchange and the Vosko−Wilk−Nusair parametrization for correlation.[69] For first row atoms, the 1s shell was frozen and described by a single Slater function. The frozen core of heavier atoms, neon-like for S and argon-like for Fe, was also modeled by a minimal

(58) Lawrence, J. D.; Li, H.; Rauchfuss, T. B. *Chem. Commun.* **2001**, 1482−1483.
(59) Lawrence, J. D.; Li, H.; Rauchfuss, T. B.; Bénard, M.; Rohmer, M.-M. *Angew Chem., Int. Ed.* **2001**, *40*, 1768−1771.
(60) Winter, A.; Zsolnai, L.; Huttner, G. *Z. Naturforsch.* **1982**, *37b*, 1430−1436.
(61) *ADF 2.3 User's Guide*; Chemistry Department, Vrije Universiteit: Amsterdam, The Netherlands, 1997.
(62) Baerends, E. J.; Ellis, D. E.; Ros, P. *Chem. Phys.* **1973**, *2*, 41−51.
(63) Te Velde, G.; Baerends, E. J. *J. Comput. Phys.* **1992**, *99*, 84−98.
(64) Fonseca-Guerra, C.; Visser, O.; Snijders, J. G.; Baerends, E. J. In *Methods and Techniques in Computational Chemistry: METECC-95*; Clementi, E., Corongiu, G., Eds.; STEF: Cagliari, Italy, 1995; pp 305−395.
(65) Becke, A. D. *Phys. Rev. A: At., Mol., Opt. Phys.* **1988**, *38*, 3098−3100.
(66) Becke, A. D. *J. Chem. Phys.* **1986**, *84*, 4524−4529.
(67) Perdew, J. P. *Phys. Rev.* **1986**, *B33*, 8822−8824.
(68) Perdew, J. P. *Phys. Rev.* **1986**, *B34*, 7406.
(69) Vosko, S. H.; Wilk, L.; Nusair, M. *Can. J. Phys.* **1980**, *58*, 1200−1211.

Slater basis. For all nonmetal atoms, the Slater basis set used for the valence shell is of triple-ζ quality and supplemented with one polarization function. The 3s and 3p shells of Fe are described by a double-ζ Slater basis, the 3d and 4s, by a triple-ζ basis, and the 4p shell is described by a single orbital.[70,71]

Preparation of 2H. A solution of 0.40 g (1.0 mmol) of $Fe_2(S_2C_3H_6)(CO)_6$ in 10 mL of MeCN at −40 °C was treated with a solution of 0.4 mL (4.0 mmol) of PMe_3 in 10 mL of MeCN followed by a solution of 0.15 g (0.95 mmol) of Et_4NCN in 5 mL of MeCN. The reaction mixture was warmed to −10 °C. After 1 h, the resulting dark red-purple solution was warmed to room temperature, and the solvent volume was reduced to 5 mL. To this solution was added 3 mL of a 3 M solution of H_2SO_4 in MeCN, followed by 60 mL of H_2O, leading to the precipitation of a red oil, which solidified after washing with 20 mL of H_2O and drying under vacuum. Yield: 0.21 g (47%). Anal. Calcd for $C_{11}H_{16}Fe_2NO_4PS_2$: C, 30.51; H, 3.72; N, 3.23. Found: C, 30.14; H, 3.37; N, 3.08. ^{1}H NMR (500 MHz, CD_3CN): δ 2.59 and 2.43 (m, 4H, SCH_2), 2.26 and 2.15 (m, 2H, $CH_2CH_2CH_2$), 1.53 (d, 9H, CH_3), −17.08 (d, J_{H-P} = 24 Hz, 1H, Fe*H*Fe). ^{31}P NMR (200 MHz, C_6D_6): δ 22.7 (d). ^{13}C NMR (126 MHz, −20 °C, CD_3CN): d 17.7 (d, $P(CH_3)_3$), 20.6 (s, $CH_2CH_2CH_2$), 21.1 (s, SCH_2), 138.4 (br, Fe*C*N), 208.7 (dd, Fe*C*O), 209.1 (dd, Fe*C*O), 209.6 (dd, Fe*C*O), 210.2 (d, Fe*C*O). IR (THF): ν_{CN} = 2117; ν_{CO} = 2047, 2023, 1991, 1975, 1943 cm^{-1}.

$(Et_4N)\{Fe_2(S_2C_3H_6)(CN)(CO)_4[P(OMe)_3]\}$ (4). A solution of 0.30 g (0.78 mmol) of $Fe_2(S_2C_3H_6)(CO)_6$ in 10 mL of MeCN at −40 °C was treated with a solution of 1.8 mL (15 mmol) of $P(OMe)_3$ followed by a solution of 0.12 g (0.78 mmol) of Et_4NCN in 5 mL of MeCN. The reaction mixture was allowed to warm to room temperature over 60 min. The resulting dark red-purple solution was evaporated to dryness under vacuum. The red oil was extracted with 15 mL of THF and filtered, leaving behind a large amount of red precipitate. The volume was reduced under vacuum to ca. 5 mL, and the product was precipitated with 30 mL of hexane as an oil, which solidified after being washed with additional hexane and drying under vacuum. Yield: ∼0.2 g (∼40%). Anal. Calcd for $C_{19}H_{35}Fe_2N_2O_7PS_2$: C, 37.39; H, 5.78; N, 4.59. Found: C, 37.00; H, 5.79; N, 4.30. ^{1}H NMR (500 MHz, CD_3CN): δ 3.79 (d, 9H, $P(OCH_3)_3$), 3.16 (q, 8H, NCH_2CH_3), 2.0 (br, 4H, SCH_2), 1.75 and 1.65 (br, 2H, $SCH_2CH_2CH_2S$), 1.198 (t, 12H, NCH_2CH_3). ^{31}P NMR (200 MHz, C_6D_6): δ 183.3 (s). IR (MeCN): ν_{CN} = 2085; ν_{CO} = 1986, 1949, 1910, 1897 cm^{-1}.

In Situ Protonation of $(Et_4N)\{Fe_2(S_2C_3H_6)(CN)(CO)_4[P(OMe)_3]\}$. A solution of 0.011 g (0.018 mmol) of $(Et_4N)\{Fe_2(S_2C_3H_6)(CN)(CO)_4[P(OMe)_3]\}$ in 1 mL of CD_3CN was treated with 0.008 g (0.04 mmol) of HOTs·H_2O. ^{1}H NMR (500 MHz, CD_3CN): δ 3.71 (d, 9H, $P(OCH_3)_3$), 3.13 (q, 8H, NCH_2CH_3), (br, SCH_2), 1.71 (br, 2H, $SCH_2CH_2CH_2S$), 1.183 (t, 12H, NCH_2CH_3). ^{31}P NMR (200 MHz, C_6D_6): δ 180.4 (s). IR (THF): ν_{CO} = 2039, 1994, 1965, 1932 cm^{-1}.

$Fe_2(S_2C_3H_6)(CNMe)(CO)_4(PMe_3)$ (2Me). A solution of 0.21 (0.37 mmol) of $(NEt_4)[Fe_2(S_2C_3H_6)(CN)(CO)_4(PMe_3)]$ in 15 mL of MeCN at 0 °C was treated with a solution of 0.055 g (0.37 mmol) of $(Me_3O)(BF_4)$ in 5 mL of MeCN. The reaction mixture was held at 0°C for 1 h and then warmed to room temperature. The resulting red solution was evaporated to dryness under vacuum. The red oil was extracted with 15 mL of THF and filtered through a 6 cm × 3 cm plug of silica, leaving behind a dark red band. The solvent was removed under vacuum, and the product was extracted with 30 mL of hexane. The solvent was removed under vacuum, giving a red oil. Yield ∼ 30 mg (20%). ^{1}H NMR (500 MHz, CD_3CN): δ 3.37 (s, 3H, $CNCH_3$), 2.08 (m, 4H, SCH_2), 1.86 (dt, 2H, $SCH_2CH_2CH_2S$), 1.43 (d, 9H, PCH_3). ^{31}P NMR (200 MHz, C_6D_6): δ 26.9 (s). IR (hexane): ν_{CNMe} = 2158; ν_{CO} = 2004(w), 1999 (w), 1991 (w), 1964 (s), 1937 (s), 1910 (s) cm^{-1}.

Acknowledgment. This research was supported by NIH and DOE. F.G. thanks the CNRS (France) for a leave of absence. We thank IDRIS (Orsay) and CURRI (Strasbourg) for computer time and Dr. Scott Wilson for assistance with the crystallography.

Supporting Information Available: CV figures (PDF), crystallographic information files (CIF), crystallographic tables (PDF). This material is available free of charge via the Internet at http://pubs.acs.org.

IC025838X

(70) Snijders, J. G.; Vernooijs, P.; Baerends, E. J. *At. Data Nucl. Data Tables* **1981**, *26*, 483−509.
(71) Vernooijs, P.; Snijders, J. G.; Baerends, E. J. *Slater type basis functions for the whole periodic table*; Free University of Amsterdam: Amsterdam, The Netherlands, 1981.